Available online at www.sciencedirect.com
SCIENCE DIRECT®
Journal of Power Sources 124 (2003) 538–550
JOURNAL OF POWER SOURCES
www.elsevier.com/locate/jpowsour

Effect of cathode composition on capacity fade, impedance rise and power fade in high-power, lithium-ion cells☆

Ira Bloom[a,*], Scott A. Jones[a], Vincent S. Battaglia[a], Gary L. Henriksen[a], Jon P. Christophersen[b], Randy B. Wright[b], Chinh D. Ho[b], Jeffrey R. Belt[b], Chester G. Motloch[b]

[a] *Electrochemical Technology Program, Argonne National Laboratory, 9700 South Cass Avenue, Argonne, IL 60439, USA*
[b] *Idaho National Engineering and Environmental Laboratory, P.O. Box 1625, Idaho Falls, ID 83415, USA*

Received 2 June 2003; received in revised form 12 June 2003; accepted 12 June 2003

Abstract

We tested the effect of Al concentration on the performance of lithium-ion cells. One set of cells contained a $LiNi_{0.8}Co_{0.15}Al_{0.05}O_2$ cathode and the other, $LiNi_{0.8}Co_{0.10}Al_{0.10}O_2$. The cells were calendar- and cycle-life tested at several temperatures, with periodic interruptions for reference performance tests that were used to gauge capacity and power fade as a function of time.

The $C_1/25$ capacity fade in the cells displayed $t^{1/2}$ dependence. The capacity fade of the 10% Al-doped cells tested at 45 °C was similar to that of the 5% Al-doped cells at 25 °C. The impedance rise and power fade were also sensitive to the Al concentration. For the one common temperature investigated (i.e., 45 °C), the 10% Al-doped cells displayed higher impedance rise and power fade than the 5% Al-doped cells. Additionally, the time dependence of the impedance rise displayed two distinct kinetic regimes; the initial portion depended on $t^{1/2}$ and the final, on t. On the other hand, the 10% Al-doped cells depended on $t^{1/2}$ only.

Keywords: Capacity fade; Impedance rise; Power fade

1. Introduction

Lithium-ion batteries have found uses in many consumer electronics. The batteries generally consist of a metal oxide cathode, a liquid organic solvent containing a dissolved ionic salt, and a carbon-based anode. The US Department of Energy-supported Partnership for the Next Generation of Vehicles (PNGV, now called the Freedom Cooperative Automotive Research, FreedomCAR, Partnership) and others are also evaluating this class of batteries for use in hybrid electric vehicles. For this use, the batteries must exhibit 23% power fade or less over 15 years. However, during their lives, these cells show impedance increase and, hence, power fade. Thus, the 15-year life remains a challenge.

The US Department of Energy's (DOE) Office of FreedomCAR and Vehicle Technologies is working in a collaborative manner with the US auto companies. DOE established a technical support program at DOE's national laboratories to address, among other issues, calendar-life. This national laboratory program is denoted the Advanced Technology Development (ATD) Program.

Under the auspices of the ATD Program, two national laboratories, Argonne National Laboratory (ANL) and Idaho National Engineering and Environmental Laboratory (INEEL), collaborated to evaluate, among other phenomena, the causes of the impedance rise in these cells. In this study, a number of 18650-sized cells containing two different chemistries, which differed in the aluminum (and cobalt) content in the cathode, were subjected to accelerated cycle- and calendar-life testing, as defined later. It was thought that the higher Al content would increase the stability of the cathode, i.e., reduce capacity fade in the cell.

Papers on impedance increase in these lithium-ion cells have appeared elsewhere [1–4]. These studies showed that the discharge impedance increase was proportional to $(\text{time})^{1/2}$, regardless of the nature of the aging experiment. The authors inferred that the most likely source of this

☆ The submitted issue has been created by the University of Chicago as Operator of Argonne National Laboratory (Argonne) under Contract No. W-31-109-Eng-38 with the US Department of Energy. The US Government retains for itself, and others acting on its behalf, a paid-up, non-exclusive, irrevocable, worldwide license in said article to reproduce, prepare derivative works, distribute copies to the public, and perform publicly and display publicly, by or on behalf of the government.

* Corresponding author. Tel.: +1-630-252-4516; fax: +1-630-252-4176.
E-mail address: bloom@cmt.anl.gov (I. Bloom).

0378-7753/$ – see front matter © 2003 Elsevier B.V. All rights reserved.
doi:10.1016/S0378-7753(03)00806-1

impedance increase was the growth of a solid electrolyte interface (SEI) layer on the surface of one or both of the electrodes.

2. Experimental

2.1. General

Two different cell chemistries were used in this work. The chemistry of Group A is given in Table 1. The chemistry of Group B was the same as that of Group A except that the cathode consisted of $LiNi_{0.8}Co_{0.1}Al_{0.1}O_2$ (10% Al doping and 10% cobalt). Both cell groups have an average active area of 846.3 cm^2, although the Group B cells have 20% less capacity. Forty-six, weld-sealed, 18650-sized cells containing Group A chemistry and thirty of Group B chemistry were fabricated by Quallion, LLC, to ANL's specifications for this work.

The battery ratings and limitations given in Table 2 were used to establish the testing protocols. The cells were tested for calendar-life at ANL and for cycle-life at INEEL.

The cells were characterized by many methods, including the $C_1/25$ capacity and hybrid pulse power characterization at the low current value (L-HPPC) [5]. The L-HPPC test was scaled to a 5*C* discharge current and a (3/4)5*C* regen current. All *C*/25 capacity and L-HPPC tests were performed using programmable testers. The cells were mounted in aluminum thermal blocks and placed within environmental chambers to maintain the temperature at target values and to minimize temperature fluctuations. After characterization at 25 °C, one cell of each chemistry was removed from testing at both ANL and INEEL. For the Group A cells, the resulting distribution of cells was 14 for cycle-life tests at 25 °C, 14 for cycle-life tests at 45 °C, 2 for calendar-life tests at 45 °C, and 14 for calendar-life tests at 55 °C. The Group B cells were tested at 45 °C with only 10 cells at ANL (calendar-life) and 14 at INEEL (cycle-life) after characterization. Further information about the tests is given in [6].

Cell potentials were used to establish state-of-charge (SOC). At the beginning of the life, the cells were discharged at the 25-h rate at 25 °C between 4.1 and 3.0 V to determine the relationship between SOC and potential. This relationship was used throughout the study. Calendar- and cycle-life testing were then performed at 60% SOC, which, based on the initial $C_1/25$ tests corresponded to 3.723 and 3.741 V for Groups A and B, respectively.

Table 1
Cell chemistry for Group A

Positive electrode	Negative electrode
8 wt.% PVDF binder (Kureha KF-1100)	8 wt.% PVDF binder (Kureha #C)
4 wt.% SFG-6 graphite (Timical)	92 wt.% MAG-10 (Hitachi)
4 wt.% carbon black (Chevron)	4.9 mg/cm^2 loading density
84 wt.% $LiNi_{0.8}Co_{0.15}Al_{0.05}O_2$ (Fuji CA1505)	35 μm-thick coating/side
8 mg/cm^2 loading density	18 μm-thick Cu current collector
35 μm-thick coating/side	
30 μm-thick Al current collector	
Electrolyte	**Separator**
1.2 M $LiPF_6$ in EC/EMC (3:7, w/w)	25 μm-thick PE Celgard separator

Table 2
Battery ratings and limitations

	Group A	Group B
C_1/1 rated capacity (Ah)	1.0	0.8
Cell nominal weight (average, g)	38.7	38.4
Temperature (°C)		
Operating range	−20 to +60 (discharge)	
Storage	10 ± 3	
Maximum (discharge)	60	
Maximum (charge)	40	
Voltage limits (V)		
Minimum discharge voltage	3.0 (18 s pulse)	
Maximum charge voltage	3.0 (continuous)	
	4.3 (10 s pulse)	
	4.1 (continuous)	
Current limits (A)		
Maximum discharge current	8.0 (18 s pulse)	
Maximum charge current	2.0 (continuous)	
	8.0 (10 s pulse)	
	1.0 (continuous)	

The L-HPPC test was used to monitor how the impedance and power capability changed as a function of time. The raw data were reduced to produce discharge and recharge (regen) area-specific impedance (ASI) and power values for each iteration of the test profile according to the following equations and Fig. 1a.

$$\text{Discharge resistance } (R_{\text{discharge}}) = \frac{\Delta V}{\Delta I} = \frac{V_{t_1} - V_{t_0}}{I_{t_1} - I_{t_0}}$$

$$\text{Regen resistance } (R_{\text{regen}}) = \frac{V_{t_4} - V_{t_3}}{I_{t_4} - I_{t_3}}$$

$$\text{Discharge ASI} = 846.3\,\text{cm}^2 \times R_{\text{discharge}}$$

$$\text{Regen ASI} = 846.3\,\text{cm}^2 \times R_{\text{regen}}$$

$$P_{\text{discharge}} = \frac{3.0(\text{OCV} - 3.0)}{R_{\text{discharge}}}$$

$$P_{\text{regen}} = \frac{4.1(4.1 - \text{OCV}_{\text{regen}})}{R_{\text{regen}}}$$

where $t_0 = 0$ s, $t_1 = 18$ s, $t_3 = 50$ s, and $t_4 = 52$ s and where the voltage and current values associated with t_0 and t_3 are taken immediately prior to the start of the pulse.

The L-HPPC profile is completed in increments of 10% DOD. Interpretation of the L-HPPC results requires that the OCV value prior to the start of each portion of the profile

be known. The OCV value prior to the discharge portion of the profile is measured but OCV_{regen} value prior to the regen portion of the profile is not available for direct measurement (due to the relaxation time require to obtain a reasonable OCV measurement). Therefore, the OCV_{regen} value is estimated using Microsoft Excel's FORECAST function as follows:

(1) measure the Ah removed values at the 10% increments;
(2) measure the OCV values at the particular 10% DOD increments;
(3) measure the Ah removed during the discharge portion of the HPPC profile;
(4) "Forecast" the OCV_{regen} value that falls between the 10% OCV values measured and the 10% Ah values measured.

Each L-HPPC pulse can be related to the corresponding amount of energy discharged to that point. A typical plot of power versus energy removed is given in Fig. 1b. The available energy at a given power level is defined as $E_{discharge} - E_{regen}$. Plotting these values as a function of power produces Fig. 1c. The dashed line in the figure has a slope equal to the ratio of the PNGV power-assist energy goal (i.e., 300 Wh) divided by the power goal plus a 30% beginning-of-life power margin (i.e., 25 kW × 1.3). The point at which the dashed line intersects the available energy curve is where the PNGV goals are optimally met for this representative cell. This intersection point is used to calculate the battery size factor (BSF) by dividing the energy at this point by the PNGV energy goal (or, alternatively dividing the power at this point by the PNGV power goal). This calculation was performed on each cell. The average

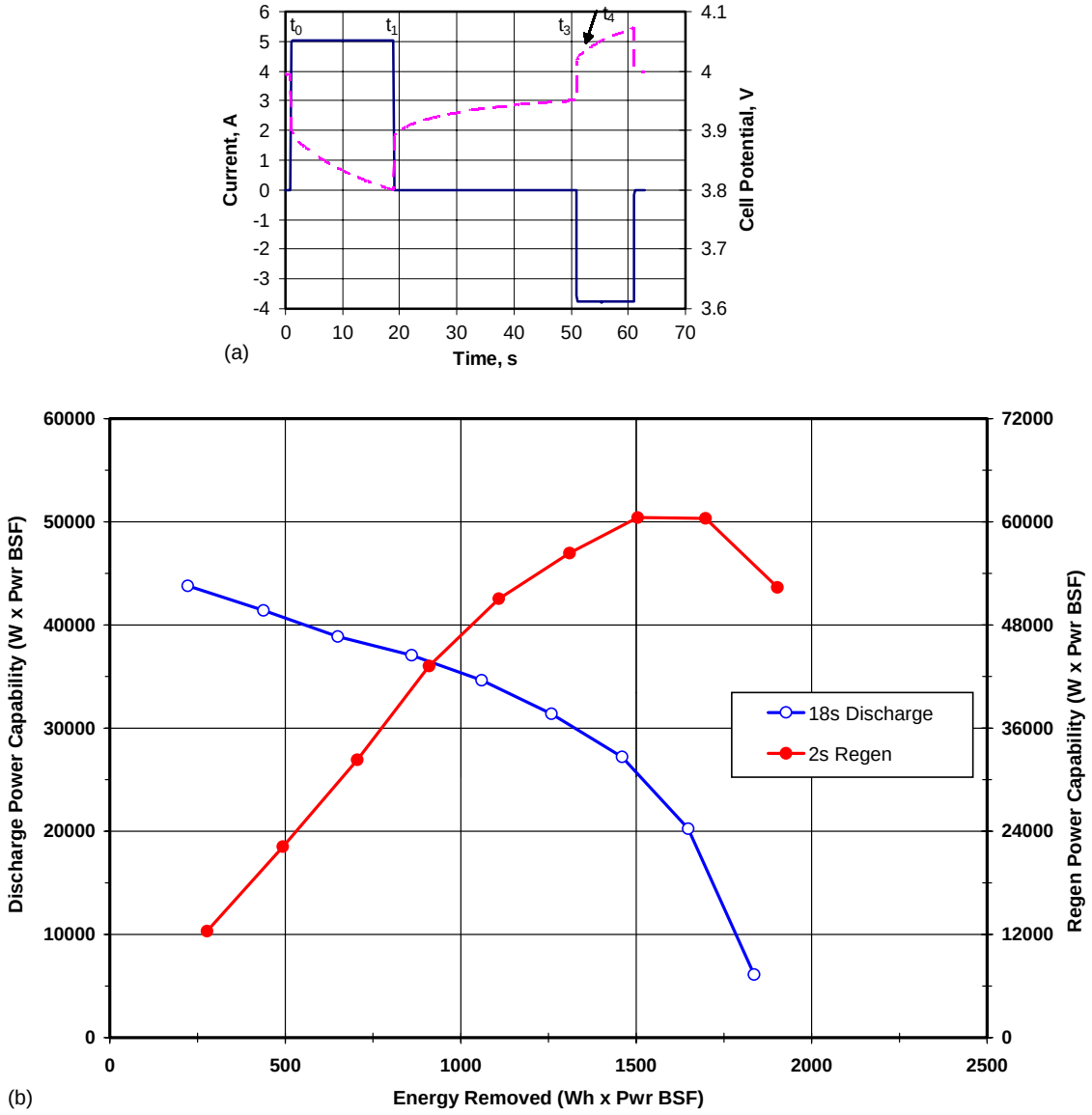

Fig. 1. (a) Cell potential and current vs. time for an L-HPPC pulse profile. Voltage is the dashed line, and current, the solid line. Discharge is defined as positive current. (b) A typical BSF-scaled discharge and regen power vs. energy removed plot. (c) A typical available energy vs. power plot.

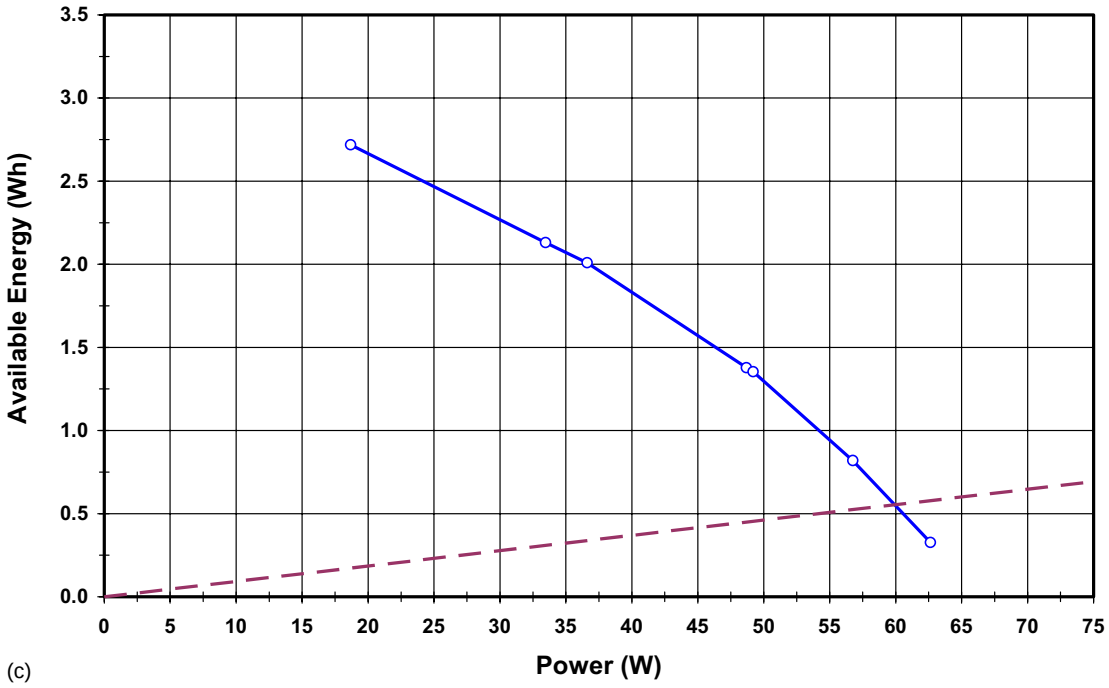

(c)

Fig. 1. (*Continued*).

BSF values for Groups A and B cells are 553 and 651, respectively. The BSF is used to scale all subsequent power and energy curves for direct comparison with the PNGV goals. The standard measure of cell degradation was the percent fade in the power at an available energy of 300 Wh. Further information about these calculations is given in [6,7].

2.2. Calendar-life tests

The Group A cells were tested for calendar-life according to the PNGV calendar test at 45 and at 55 °C. Here, the profile given in Fig. 2 is applied once per day for 28 consecutive days using the 3*C* rate as the base current [5].

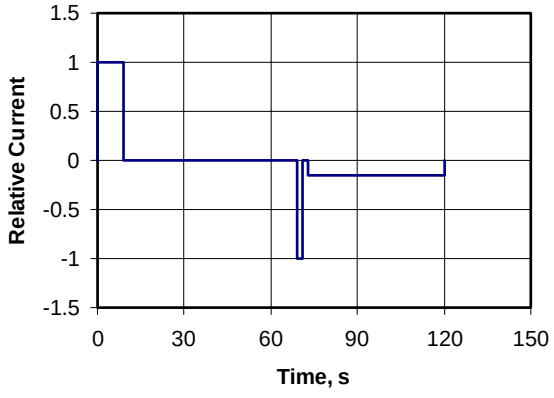

Fig. 2. Calendar-life test profile. Discharge is defined as positive current.

2.3. Reference performance tests

After 4 weeks at temperature, the cells were cooled to 25 °C and reference performance tests (RPTs) were performed. The RPT consisted of portions of the characterization tests, including the *C*/25 and L-HPPC tests. The cells were then heated back to the soak temperature. The process was repeated until the power fade at the 300 Wh line was greater than 30% for the cells at 55 °C and 50% for those at 45 °C.

The Group B cells were tested analogously. They were tested using the same test profile and procedures except that the soak temperature was 45 °C. These cells were tested until the power fade at the 300 Wh line was 50%. Following 4 weeks of aging, another two cells were removed from testing. The remaining cells were removed from the testing based on roughly equal power fade increments. Further information can be found in Appendix C of [7].

2.4. Cycle-life tests

The cells were tested for cycle-life by using the BSF-scaled, 25 Wh profile shown in Fig. 3 [5]. Before cycle-life testing, the operating set point stability (OSPS) test was performed to verify cycling stability. The OSPS test consists of 100 consecutive cycle-life profiles. The requirement is that at its completion, the actual SOC should be within ±2% of 60% SOC, based on the OCV following a 1 h rest at the beginning and end of the 100 pulses. If the SOC is charge positive or charge negative (i.e., unstable), then the control voltage at the end of the discharge pulse is

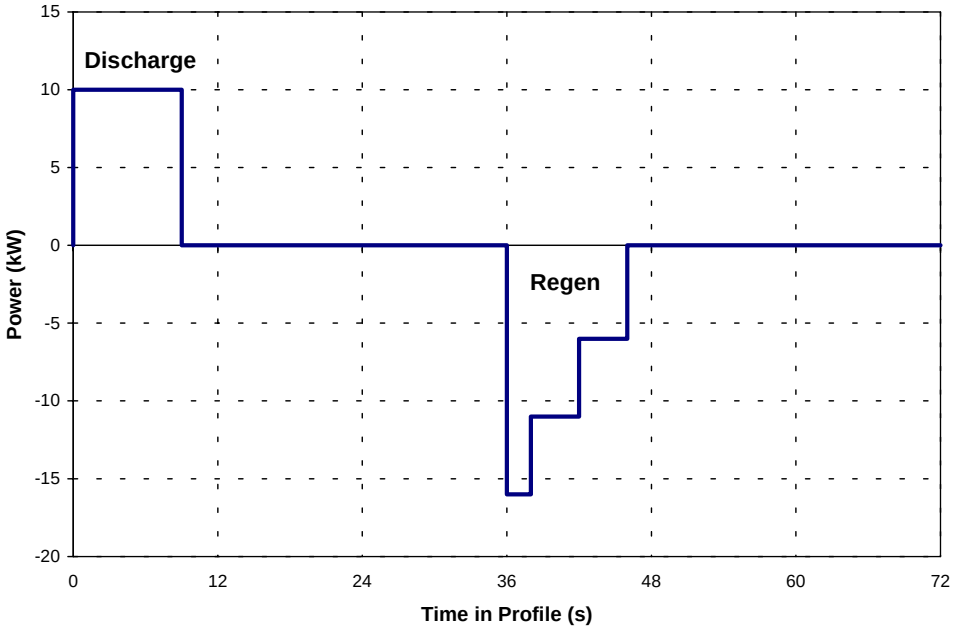

Fig. 3. 25-Wh profile used in the cycle-life tests.

changed and the OSPS test is repeated until stable cycling occurs [6].

The Group A cells were tested at 25 and 45 °C. After 4 weeks at temperature (33,600 profiles), RPTs were performed, as described earlier. Again, the Group B cells were tested analogously, except for using only one temperature, 45 °C.

2.5. Data reduction

The capacity and derived L-HPPC impedance and power values from the two test labs were pooled and analyzed for trends. The impedance at 60% SOC from the L-HPPC test was selected for analysis because it corresponds to the nominal SOC anticipated for hybrid electric vehicle operation. Where necessary, the value at 60% SOC was approximated by linear interpolation using the FORECAST function in Microsoft Excel. Outliers were identified and excluded from further calculations.

Due to the limited number of test temperatures used in these experiments, no analyses for temperature dependence were performed. However, both capacity and power fade were observed to increase with temperature, as expected. The nature of the time dependency of the impedance and static capacity changes was determined by curve fitting. For this work, equations based on time, t or $t^{1/2}$ were used. For simple equations, the Microsoft Excel function LINEST was used to determine which form of the equation produced a better fit based upon maximizing the regression coefficient, r^2. For more complex, non-linear equations, such as $at^{1/2} + c(t - t_0) + d$, where a, c, d, and t_0 are constants ($c = 0$ when $t < t_0$), the non-linear regression function in Jandel SigmaStat was used. All values of r^2 were 0.92 or better.

3. Results

The average initial discharge data and standard deviations for the cell populations are given in Table 3. For Group A, the calendar-life cells at 55 °C were tested for 40 weeks; those at 45 °C, for 76 weeks. The cycle-life cells at 25 and 45 °C were tested for 68 weeks. For Group B, the calendar-life cells were tested for 60 weeks and the cycle-life cells, for 56 weeks. In the calendar-life test, the cells at 55 °C exhibited higher capacity fade and impedance increase than did the cells tested at 45 °C. The same trend held in the cycling

Table 3
Initial values for the cell populations tested

Cell population	$C/25$ capacity (Ah)	ASI ($\Omega\,cm^2$)	Power (kW)
Group A cycle-life at 25 °C	1.08 ± 0.01	28.35 ± 0.78	32.45 ± 0.79
Group A cycle-life at 45 °C	1.07 ± 0.01	28.64 ± 0.70	32.42 ± 0.67
Group A calendar-life at 45 °C	1.02 ± 0.01	26.59 ± 0.54	35.39 ± 0.65
Group A calendar-life at 55 °C	1.03 ± 0.03	28.00 ± 1.69	33.74 ± 2.36
Group B cycle-life	0.98 ± 0.03	33.86 ± 0.78	32.57 ± 1.06
Group B calendar-life	0.96 ± 0.01	31.40 ± 0.82	34.11 ± 2.29

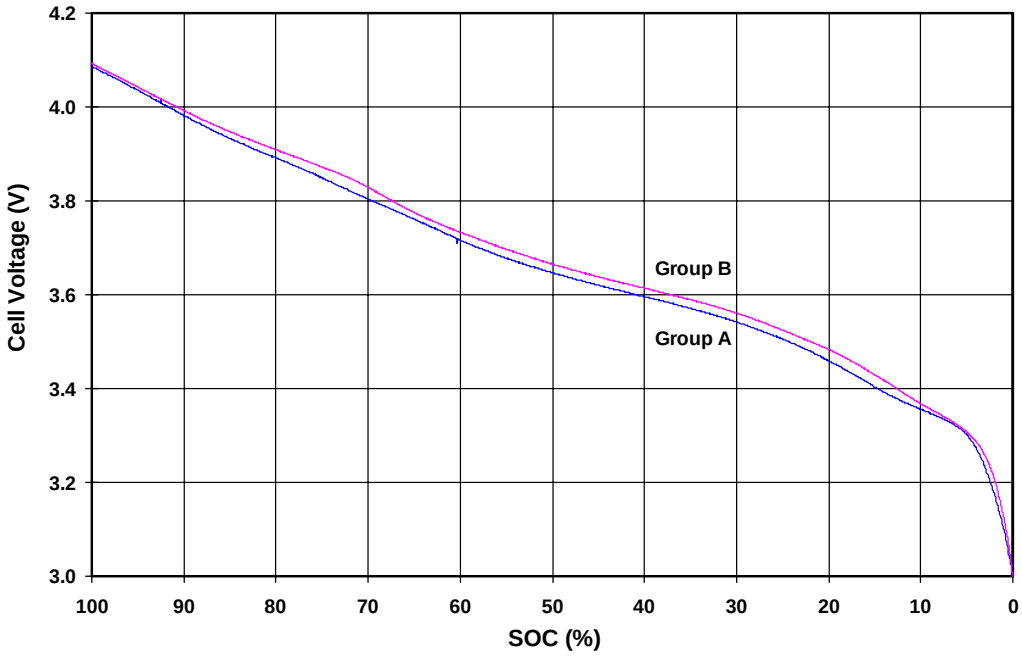

Fig. 4. Discharge cell voltage vs. %SOC for cell Groups A and B at characterization.

test. The cells cycled at 45 °C exhibited higher capacity fade and impedance increase than those tested at 25 °C. For the sake of simplicity, only the discharge-based data will be presented; the trends in the regen-based data are similar.

3.1. Capacity fade

Fig. 4 shows that the 25 h discharge curves of Groups A and B differ at the beginning of life. From the figure, the Group B cells operate at higher potentials in the %SOC range of 90 to 10. The difference at 50% SOC is approximately 17 mV and can be attributed to the difference in cathode composition.

As the cells age, the *C*/25 capacity fades. A plot of the average *C*/25 capacity versus time for the cells along with the least squares fit to $at^{1/2} + d$ is given in Fig. 5. The coefficients of these curves, their respective values of r^2 and the standard error (S.E.) for each coefficient are given in

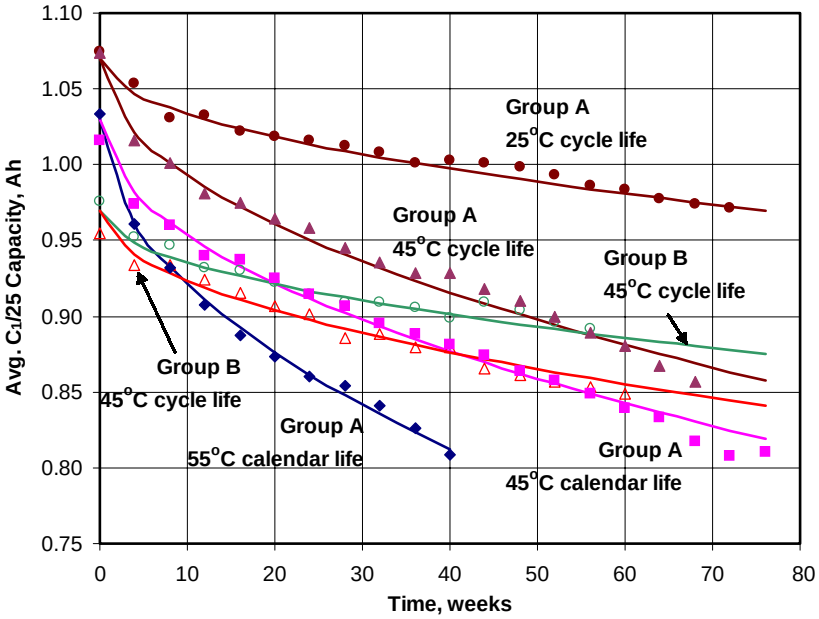

Fig. 5. Average C_1/25 capacity as a function of time.

Table 4
Coefficients, S.E. and values of r^2 for the curves in Fig. 5

	Coefficient		
	a	d	r^2
Group A cycle-life 25 °C	-1.15×10^{-2}	1.07	0.98
S.E.	3.87×10^{-4}	2.32×10^{-3}	
Group A cycle-life 45 °C	-2.44×10^{-2}	1.07	0.99
S.E.	7.14×10^{-4}	4.16×10^{-3}	
Group A calendar-life 45 °C	-2.42×10^{-2}	1.03	0.99
S.E.	6.78×10^{-4}	4.18×10^{-3}	
Group A calendar-life 55 °C	-3.44×10^{-2}	1.03	1.00
S.E.	6.53×10^{-4}	2.92×10^{-3}	
Group B cycle-life 45 °C	-1.09×10^{-2}	0.97	0.97
S.E.	5.69×10^{-4}	3.01×10^{-3}	
Group B calendar-life 45 °C	-1.48×10^{-2}	0.97	0.96
S.E.	7.53×10^{-4}	4.12×10^{-3}	

Table 4. From the values of r^2, the fits are excellent. The "a" column in Table 4 shows that the order of $C/25$ capacity fades is 55 °C calendar-life > Group A cycle-life at 45 °C ∼ Group A calendar-life at 45 °C > Group B calendar-life at 45 °C = Group B cycle-life at 45 °C ∼ 25 °C cycle-life.

The fact that the cells at the highest temperature, 55 °C, have the highest capacity fade is expected. This effect of temperature has been documented in earlier studies on lithium-ion cells [1,4]. The results also show that cycling affects capacity fade, but only slightly. The relatively small difference in fade rate (values of a) between the calendar-life cells and the cycle-life cells may be a result of the mild nature of the cycling which utilized pulses of less than ±2% ΔSOC swing.

The effect of the higher Al content in the Group B cells can clearly be seen. There is no significant difference between the Group B cells (cycle- or calendar-life) tested at 45 °C and the Group A cells cycled at 25 °C. Thus, the higher Al content stabilizes the cathode towards against loss.

Capacity loss indicates that some process is impeding the retention or use of all the electrochemically active lithium. As can be seen in Table 4, the regression coefficients for the data indicate that the average $C_1/25$ capacity decrease depends on $t^{1/2}$. Indeed, parabolic models of capacity decline have been reported by Broussely et al. [8]. Broussely et al. fit their capacity data to equations of the general form, $t = k_1x^2 + k_2x$, where x is the percent lithium (i.e., capacity) loss and k_1 and k_2 are constants. They attribute the capacity fade to a lithium corrosion reaction that occurs between the anode and the electrolyte.

In the ATD work, similar, though simpler, equations ($t = kx^2 + c$) were used to describe the data with reasonable fits. Although there is no direct evidence of the capacity fade being caused by one electrode or the other, the data are consistent with those of Broussely et al. It is interesting to note (see Fig. 5) that at time greater than 60 weeks, there is a deviation from $t^{1/2}$ dependence. This could be due to another lithium-consuming reaction or process.

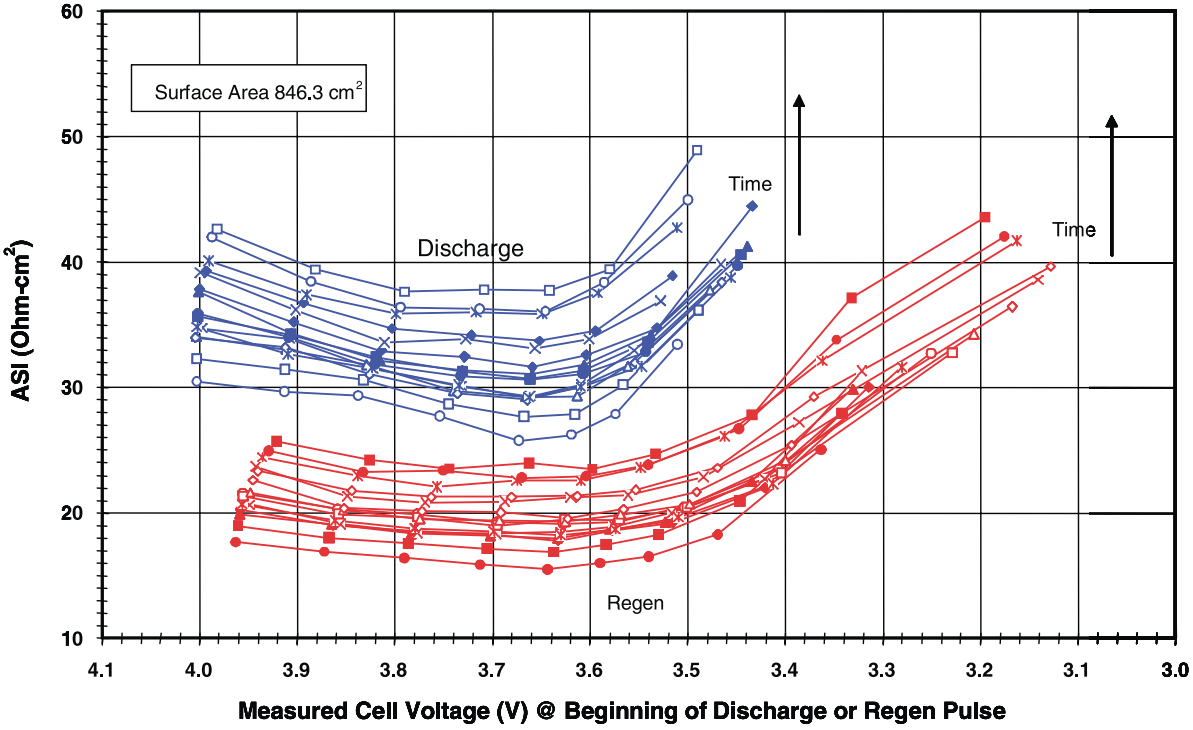

Fig. 6. Typical ASI as a function of cell voltage for Group A (60% SOC = 3.723 V). The time difference between consecutive curves is 4 weeks. As the cell ages, the ASI of the cell for both discharge and regen increases.

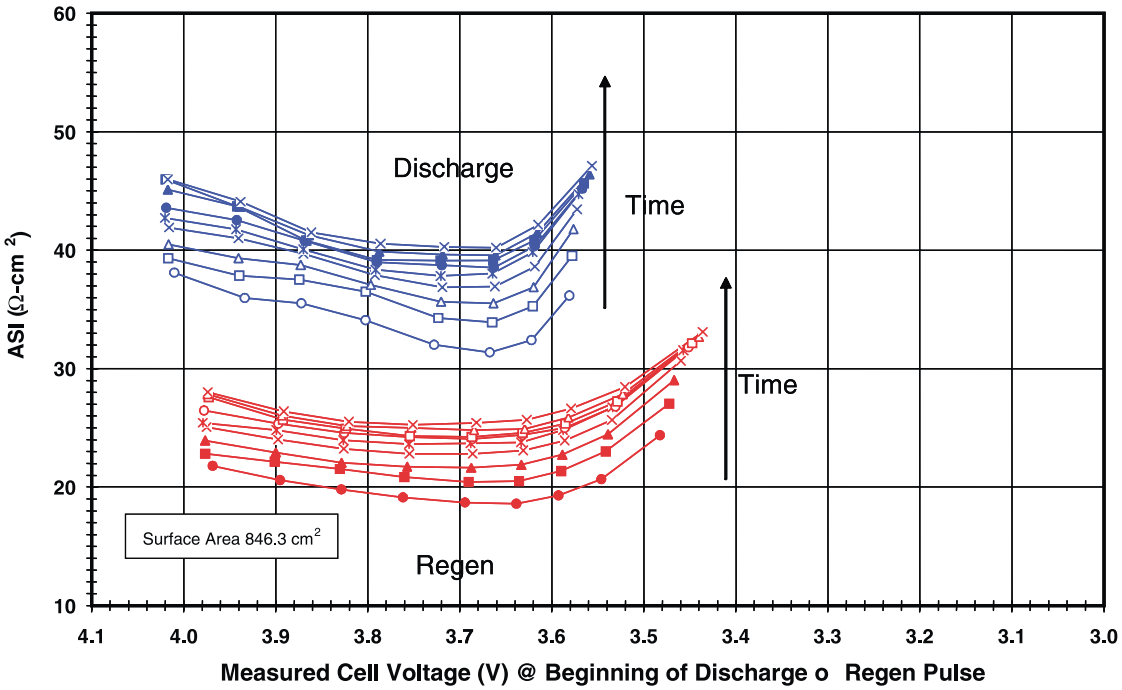

Fig. 7. Typical ASI as a function of SOC for Group B (60% SOC = 3.741 V). The time difference between consecutive curves is 4 weeks. As the cell ages, the ASI of the cell for both discharge and regen increases.

3.2. Impedance rise

The ASI values, as defined earlier, increased with time during the test. Fig. 6 shows a typical L-HPPC-derived ASI versus OCV plot for a Group A calendar-life cell. Note that the discharges resulting in the cell hitting the minimum defined cell voltage are not included in the graph. The corresponding plot from a Group B calendar-life cell is given in Fig. 7. From these figures, one can see that the initial ASI values for the Group A cells were lower than those of Group B.

Plotting the average ASI values at 60% SOC yields Fig. 8. Here, several trends are seen. In the Group A cells, the discharge ASI follows expected trends. That is, the calendar-life ASI at 55 °C > cycle-life ASI at 45 °C > calendar-life ASI at 45 °C > cycle-life ASI at 25 °C. Group B displays a similar trend. The ASI in the cycle-life cells is greater than that of the calendar-life cells. Comparing Groups A and B shows that the initial average ASI of Group B was greater than that of Group A.

Additionally, a break in the ASI versus time curves from the Group A cells at 25, 45 and 55 °C is seen. After about 44 weeks at 25 °C, after about 36 weeks at 45 °C and after about 20–24 weeks at 55 °C, the time dependence of impedance increase changes from $t^{1/2}$ to t. As expected, the break in the curve at 25 °C occurs much later in cell life than at 45 or 55 °C. Both calendar- and cycle-life Group B cells display $t^{1/2}$ dependency only.

The ASI data from the Group A cycle-life cells at 25 °C, those from the calendar- and cycle-life cells at 45 °C and those from the calendar-life cells at 55 °C were fit to the non-linear equation, $at^{1/2} + c(t - t_0) + d$, where $c = 0$ when $t < t_0$. The values of the constants, a, c, d, and t_0, and their respective values of r^2 are given in Table 5. The values of r^2 show that the fits are excellent.

From the data in Table 5, the values of a for the Group A cells calendar- and cycle-life tested at 45 °C are different within the error of the fit. This implies the initial rates of ASI increase, $at^{-1/2}/2$ ($t < t_0$), are different. Thus, cycle-life testing causes a greater rate of ASI increase than

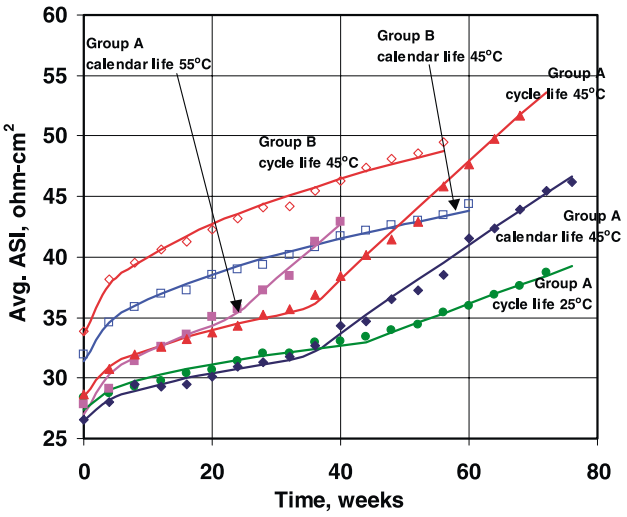

Fig. 8. Discharge ASI at 60% SOC vs. time as a function of time for the cells. The experimental data are represented as markers.

Table 5
Values of a, c, d, t_0 and r^2 for fits of ASI vs. time shown in Fig. 8

	Values				r^2	S.E.			
	a	c	d	t_0		a	c	d	t_0
Group A cycle-life 25 °C	0.85	0.14	27.34	44.30	0.98	0.07	0.02	0.31	2.88
Group A cycle-life 45 °C	1.23	0.40	28.46	35.15	1.00	0.08	0.01	0.34	0.90
Group A calendar-life 45 °C	0.89	0.30	26.44	34.48	0.99	0.10	0.01	0.39	1.39
Group A calendar-life 55 °C	1.63	0.31	27.04	22.78	0.99	0.19	0.06	0.60	2.43
Group B calendar-life 45 °C	1.60		31.99		0.99	0.04		0.22	
Group B cycle-life 45 °C	2.03		33.60		0.99	0.06		0.30	

does calendar-life testing. Similar to the initial rates in Group A, rates of ASI increase for Group B are different. The effect of test type is also seen in Group B.

There are apparently two mechanisms operating in the Group A, one that is $t^{1/2}$-based and one that is not. Time and temperature determine which one is the major contribution to the increase in cell impedance. At 45 and 55 °C, the change occurs fairly quickly. At 25 °C, the change occurs later.

3.3. Power fade

A typical available energy versus power plot for a Group A calendar-life cell is given in Fig. 9. The analogous plot for a Group B calendar-life cell is given in Fig. 10. Both plots show that, as expected, power fades with test time (see Fig. 11).

One would expect that the power capability of a cell to depend on its ASI. Since power, P, decreases as ASI increases, $P \propto 1/\text{ASI}$. Plotting $1/P$ versus time should yield curves with similar shapes as those seen in the plots of ASI versus time.

Fig. 12 gives the plot of the reciprocal of average power at 300 Wh. Similar to that seen in Fig. 8, a break in the curves from the Group A cells at 45 and 55 °C is seen. After about 37–38 weeks at 45 °C, after about 24 weeks at 55 °C, and after about 44 weeks at 25 °C, the time dependence of impedance increase changes from $t^{1/2}$ to t. Both calendar- and cycle-life Group B cells display $t^{1/2}$ dependency only.

The data from the Group A cycle-life cells at 25 °C, those from the Group A calendar- and cycle-life cells at 45 °C, and those from the Group A calendar-life cells at 55 °C were fit to the non-linear equation, $at^{1/2} + c(t - t_0) + d$, where $c = 0$ when $t < t_0$. The reciprocal power data from Group B calendar- and cycle-life cells were fit to the equation, $at^{1/2} + d$. The values of the constants, a, c, d, and t_0, and their respective values of r^2 are given in Table 6. The values of r^2 show that the fits are excellent.

Inspection of Fig. 12 shows that, at 32 weeks, the order of increasing power fade is Group A cycle-life at 25 °C <

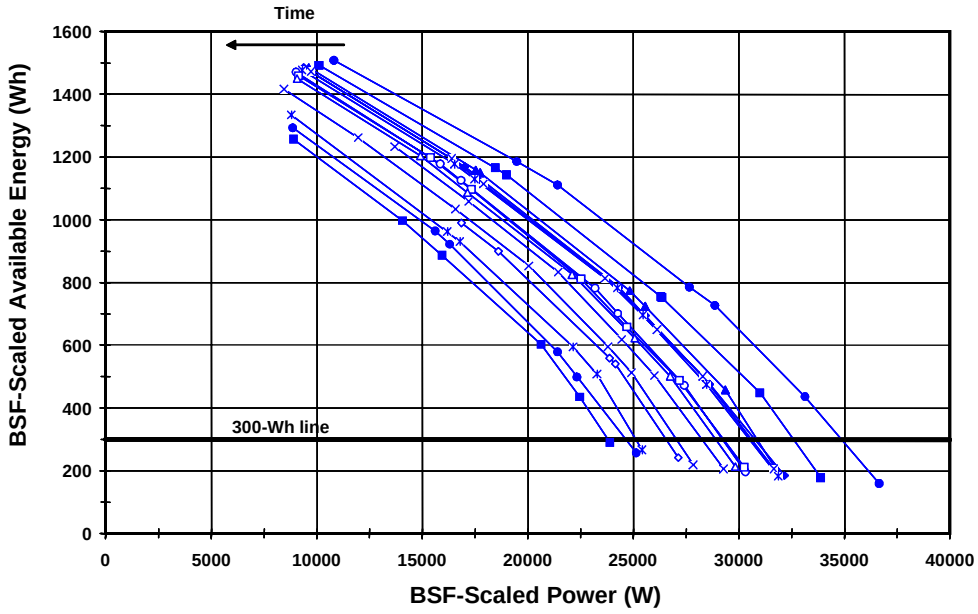

Fig. 9. Typical available energy vs. power plots for a Group A calendar-life cell (45 °C). The time difference between consecutive curves is 4 weeks. As the cell ages, the available energy at a given power decreases and the curve shifts to the left.

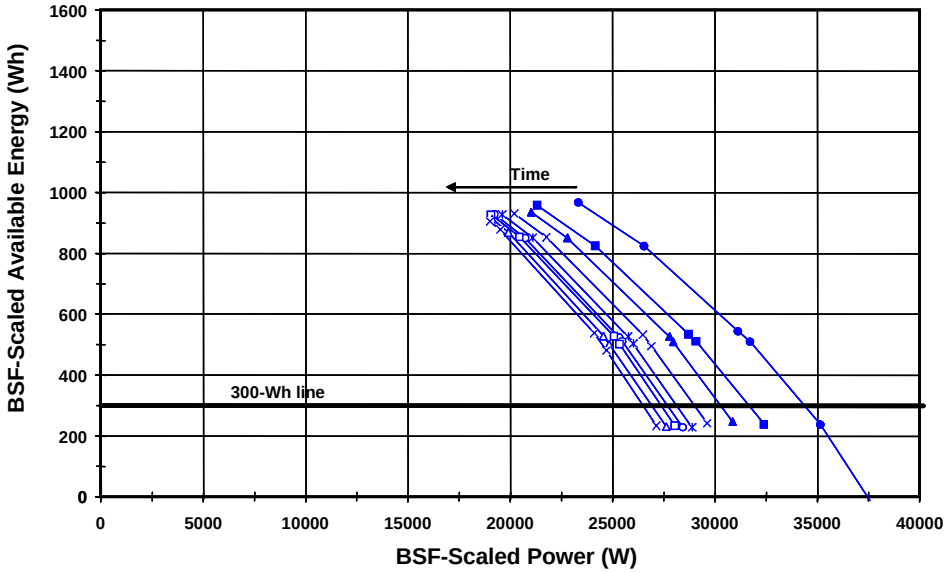

Fig. 10. Typical available energy vs. power plots for a Group B calendar-life cell (45 °C). The time difference between consecutive curves is 4 weeks. As the cell ages, the available energy at a given power decreases and the curve shifts to the left.

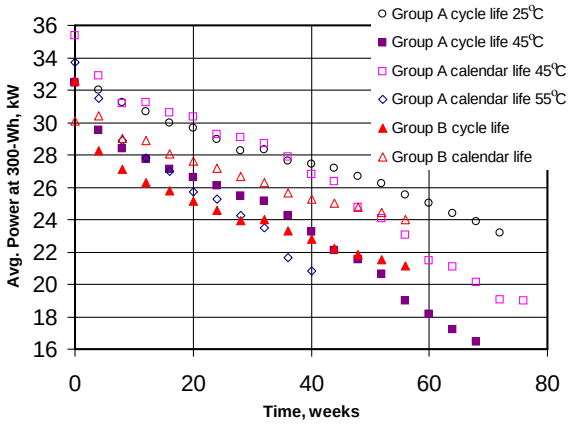

Fig. 11. Average power at 300 Wh vs. time.

Group A calendar-life at 45 °C ∼ Group B calendar-life < Group A cycle-life at 45 °C < Group B cycle-life < Group A calendar-life at 55 °C. It should be noted that this order is time dependent; the curves cross at later times.

Comparing Fig. 12 with Fig. 8 shows that, in general, the trends in power follow the trends in impedance. If the impedance curve in Fig. 8 has a transition from $t^{1/2}$ to t, the power curve does also. Comparing the values of a for all but the 25 °C cells shows the effect of the test type and cathode composition on $1/P$ versus time. The Group A cycle- and calendar-life cells at 45 °C have a small, but statistically significant difference in the value of a, which may indicate the added stress due to life cycling. The same observation can be made for the Group B cells.

4. Discussion

In the literature, the growth of a thin film, e.g. SEI layer, can be proportional to $t^{1/2}$ [1,9,10]. Square-root-of-time dependent (parabolic kinetics), as well as linear-with-time, kinetic mechanisms have been found for the growth of an oxide film on a metal surface [11–16]. The square-root-of-time dependent mechanisms tend to have a strong diffusion component and follow Arrhenius-like temperature dependence. In the linear-with-time case, the rate of oxidation is constant with time and is thus independent of the amount of gas or metal previously consumed in the formation of

Table 6
Values of a, c, d, t_0 and r^2 for fits of $1/P$ vs. time shown in Fig. 12

	Values				r^2	S.E.			
	a ($\times 10^{-3}$)	c ($\times 10^{-4}$)	d ($\times 10^{-2}$)	t_0		a ($\times 10^{-4}$)	c ($\times 10^{-5}$)	d ($\times 10^{-4}$)	t_0
Group A cycle-life 25 °C	1.02	1.72	2.97	45.00	0.99	0.71	0.22	3.33	2.52
Group A cycle-life 45 °C	1.64	5.38	3.06	37.91	1.00	1.15	2.59	4.84	1.06
Group A calendar-life 45 °C	1.19	3.86	2.82	37.94	1.00	1.02	1.71	4.34	1.22
Group A calendar-life 55 °C	2.06	3.64	2.89	23.63	0.99	2.11	6.34	6.68	2.25
Group B cycle-life 45 °C	15.66		2.90		0.98	0.58		3.16	
Group B calendar-life 45 °C	21.38		3.06		0.99	0.61		3.20	

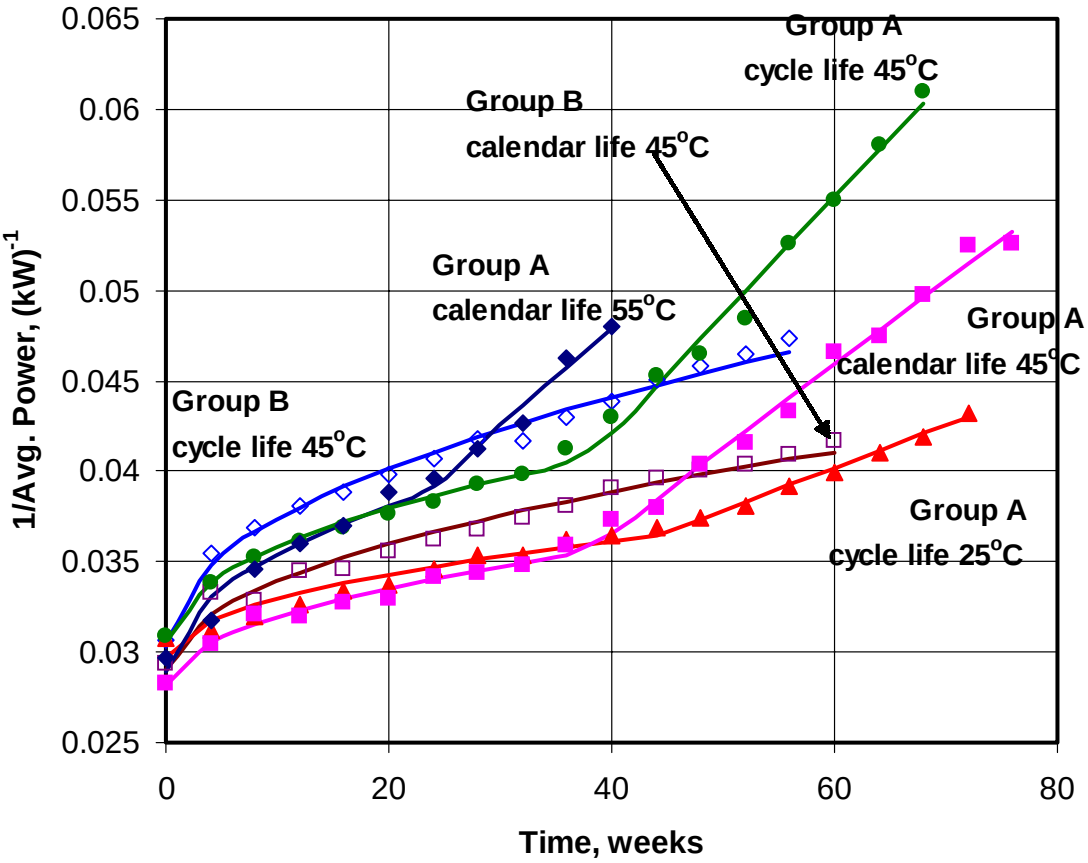

Fig. 12. 1/Power at the 300 Wh line vs. time. The data points are represented by markers.

the oxide layer. The linear growth law has been found to describe metal oxidation reactions whose rate is controlled by a surface reaction step.

Applying this analogy to the Li-ion battery case, the formation of a thin film on a Li-ion battery electrode may occur in much the same manner as an oxide film on a metal. It is possible that the reaction of the electrolyte with an electrode to form species, such as lithium alkoxides, lithium carbonates, or LiF, follows parabolic kinetics. For the linear section, the reaction mechanism and/or products may have changed. Another possibility is that the surface film no longer protects the electrode surface due to cracks or fractures in the surface film arising from charge and/or temperature cycling. These types of behaviors have been reported in the literature in the oxidation of Fe [17], Nb [18,19], and Ce [20].

If the SEI layer grows similar to scales on Fe or Nb (see Fig. 13), the oxide layer initially grows with $t^{1/2}$ from (a) to (b). Here, a compact layer is growing; the impedance of which is proportional to its thickness. With time, there is a change in mechanism, as illustrated by going from (b) to (c). The route has a change in scale morphology, the morphology changes from compact to porous, as in NbO/NbO_2. However, this scenario would produce a smooth transition from $t^{1/2}$ to t, a paralinear kinetic rate law [21]. There would be no sharp break in the ASI curve (see Fig. 14).[1]

In our case, it is more likely that the source of capacity fade and impedance rise involves both electrodes. For example, if the source of capacity fade and impedance increase were at the anode initially, then the parabolic relationship in ASI increase is consistent with an SEI layer growing on that electrode. At some point, the cathode becomes the major source of cell impedance due to lost available lithium capacity. The lost capacity could be from loss of particle/particle contact or material degradation. The linear portion of the

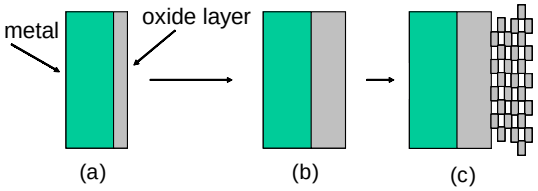

Fig. 13. A possible scenario for scale growth.

[1] The curve was calculated using the equation given in [21],

$$x = \frac{K_p}{K_l} \ln \frac{K_p}{K_p - K_l(x - K_l t)}$$

where x is the layer thickness, K_p is the parabolic reaction rate constant, K_l is the linear reaction rate constant and t is time. In the figure, $K_p = 10$ and $K_l = 0.1$.

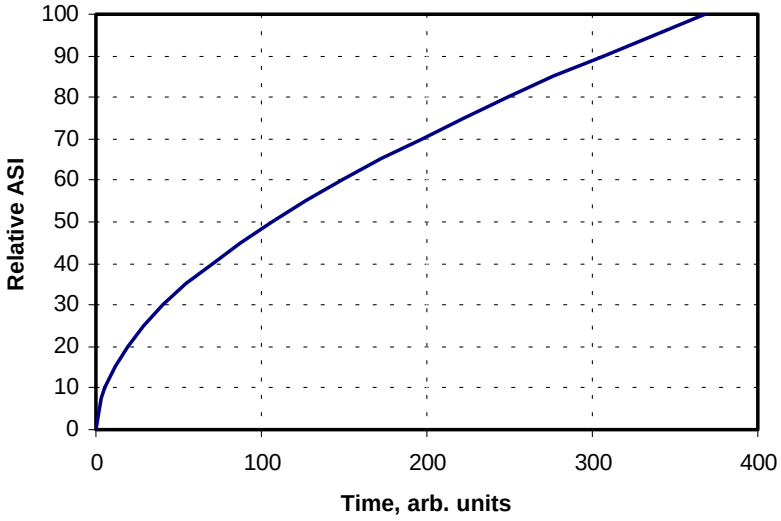

Fig. 14. Calculated ASI vs. time relationship, assuming paralinear rate law and ASI ∝ SEI layer thickness (see footnote).

curve, thus, represents the contribution of the cathode to total cell impedance. The rate of the performance-degrading process at the cathode may be controlled by a surface reaction step. The fact that the Group B cells do not show t dependence suggests that the additional Al prevents this cathode degradation process.

Taking the capacity fade and impedance increase trends together, we see that there is an initial, diffusion-limited, lithium-consuming reaction that does not change. It remains proportional to $t^{1/2}$ (for cells tested at 45 and 55 °C). On the other hand, the source of impedance increase changes with time. Initially, the rate of increase depends on the rate of lithium diffusion. With time, the Li diffusion process is no longer the rate-determining step for layer growth or impedance increase.

5. Conclusions

We tested lithium-ion cells with two different cathode compositions. One cathode contained $LiNi_{0.8}Co_{0.15}Al_{0.05}O_2$ and the other, $LiNi_{0.8}Co_{0.10}Al_{0.10}O_2$. The $C/25$ capacity fade in both types of cells displayed $t^{1/2}$ dependence. The capacity fade of the 10% Al-doped cells tested at 45 °C was similar to that of the 5% Al-doped cells at 25 °C.

The impedance rise and power fade were also sensitive to the Al concentration. The 10% Al-doped cells displayed higher impedance rise and power fade at 45 °C than the 5% Al-doped cells, but the fade rate was less. Additionally, the time dependence of the impedance rise displayed two distinct kinetic regimes; the initial portion depended on $t^{1/2}$ and the latter portion on t. On the other hand, for the 10% Al-doped cells the rate law for impedance increase was simpler and depended on $t^{1/2}$ only. While the higher Al content improved the stability of the cathode, it was detrimental to the cell impedance.

Acknowledgements

This work was performed under the auspices of the US Department of Energy, FreedomCAR and Vehicle Technologies Program, under Contract No. W-31-109-Eng-38 (ANL) and Contract No. DE-AC07-99ID13727 (INEEL).

References

[1] I. Bloom, B.W. Cole, J.J. Sohn, S.A. Jones, E.G. Polzin, V.S. Battaglia, G.L. Henriksen, C. Motloch, R. Richardson, T. Unkelhaeuser, H.L. Case, J. Power Sources 101 (2001) 238–247.
[2] R.B. Wright, C.G. Motloch, J.R. Belt, J.P. Christophersen, C.D. Ho, R.A. Richardson, I. Bloom, S.A. Jones, V.S. Battaglia, G.L. Henriksen, T. Unkelhaeuser, D. Ingersoll, H.L. Case, S.A. Rogers, R.A. Sutula, J. Power Sources 110 (2002) 445–470.
[3] I. Bloom, S.A. Jones, E.G. Polzin, V.S. Battaglia, G.L. Henriksen, C.G. Motloch, R.B. Wright, R.G. Jungst, H.L. Case, D.H. Doughty, J. Power Sources 111 (2002) 152–159.
[4] K. Amine, C.H. Chen, J. Liu, M. Hammond, A. Jansen, D. Dees, I. Bloom, D. Vissers, G. Henriksen, J. Power Sources 97–98 (2001) 684–687.
[5] PNGV Battery Test Manual, Revision 3, DOE/ID-10597, February 2001.
[6] J.P. Christophersen, C.G. Motloch, I.D. Bloom, V.S. Battaglia, E.P. Roth, T.Q. Duong, Advanced Technology Program for Lithium-Ion Batteries: Gen 2 Performance Evaluation Interim Report, February 2003, INEEL/EXT-03-00095.
[7] PNGV Test Plan for Advanced Technology Development Gen 2 Lithium Ion Cells, EHV-TP-121, Revision 6, 5 October 2001.
[8] M. Broussely, S. Herreyre, P. Biensan, P. Kasztejna, K. Nechev, R.J. Staniewicz, J. Power Sources 97–98 (2001) 13–21.
[9] E. Strauss, D. Golodnitsky, E. Peled, Electrochem. Solid State Lett. 2 (1999) 115–117.
[10] G. Blomgren, J. Power Sources 81–82 (1999) 112–118.
[11] N. Birks, G.H. Meier, Introduction to High Temperature Oxidation of Metals, Arnold, London, 1983.
[12] Per Kofstad, High-Temperature Oxidation of Metals, Wiley, New York, 1966.
[13] K. Hauffe, Oxidation of Metals, Plenum Press, New York, 1965.

[14] W. Jost, Diffusion in Solids, Liquids and Gases, Addendum, third ed., Academic Press, New York, 1960.
[15] J. Crank, The Mathematics of Diffusion, second ed., Clarendon Press, Oxford, 1975.
[16] Per Kofstad, Nonstoichiometry, Diffusion, and Electrical Conductivity in Binary Metal Oxides, Wiley, New York, 1972.
[17] D.W. Juenker, R.A. Muessner, C.E. Birchenall, Corrosion 14 (1958) 57–64.
[18] T. Hurlen, J. Inst. Metals 89 (1960-61) 273–280.
[19] B. Cox, T. Johnston, Trans. Met. Soc. AIME 227 (1963) 36–47.
[20] J. Loriers, Comptes Rendus 229 (1949) 547–549.
[21] E.W. Haycock, J. Electrochem. Soc. 106 (1959) 771–775.